Mon. Not. R. Astron. Soc. **000**, 1–9 (2012) Printed 24 July 2012 (MN LaTeX style file v2.2)

arXiv:1207.5315v1 [astro-ph.GA] 23 Jul 2012

Dense Cloud Formation and Star Formation in a Barred Galaxy

M. Nimori[1], A. Habe,[1], K. Sorai[1],Y. Watanabe[2], A. Hirota[3], and D. Namekata[4]
[1]*Department of Physics, Graduate School of Science,Hokkaido University, Kita 10 Nishi 8, Kita-ku, Sapporo, 060-0810, Japan*
[2]*Department of Physics, Graduate School of Science, The University of Tokyo, 7-3-1 Hongo, Bunkyo-ku, Tokyo 113-0033, Japan*
[3] *Nobeyama Radio Observatory, 462-2 Nobeyama, Minamimaki, Minamisaku, Nagano 384-1305, Japan*
[4]*Center for Computational Science, University of Tsukuba, 1-1-1, Tennodai, Tsukuba, Ibaraki 305-8577, Japan*

Released 2012 Xxxxx XX

ABSTRACT

We investigate the properties of massive, dense clouds formed in a barred galaxy and their possible relation to star formation, performing a two-dimensional hydrodynamical simulation with the gravitational potential obtained from the 2Mass data from the barred spiral galaxy, M83. Since the environment for cloud formation and evolution in the bar region is expected to be different from that in the spiral arm region, barred galaxies are a good target to study the environmental effects on cloud formation and the subsequent star formation. Our simulation uses for an initial 80 Myr an isothermal flow of non-self gravitating gas in the barred potential, then including radiative cooling, heating and self-gravitation of the gas for the next 40 Myr, during which dense clumps are formed. We identify many cold, dense gas clumps for which the mass is more than $10^4 M_\odot$ (a value corresponding to the molecular clouds) and study the physical properties of these clumps. The relation of the velocity dispersion of the identified clump's internal motion with the clump size is similar to that observed in the molecular clouds of our Galaxy. We find that the virial parameters for clumps in the bar region are larger than that in the arm region. From our numerical results, we estimate star formation in the bar and arm region by applying the simple model of Krumholz & McKee (2005). The mean relation between star formation rate and gas surface density agrees well with the observed Kennicutt-Schmidt relation. The SFE in the bar region is three times smaller than that in the spiral region. This trend is consistent with observations of barred galaxies.

Key words: galaxies: ISM - galaxies: star formation - ISM: clouds - galaxies: structure - galaxies: kinematics and dynamics

1 INTRODUCTION

Star formation (SF) is one of the key processes governing the evolution of galaxies. Many observations of nearby disk galaxies indicate an empirical relation between gas surface density (Σ_{gas}) and star formation rate surface density (Σ_{SFR}). This relation is called the Kennicutt-Schmidt (K-S) relation (Schmidt (1959), Kennicutt (1998)). Bigiel et al. (2008) show that Σ_{SFR} is well correlated with the hydrogen molecular surface density (Σ_{H_2}) for local spiral galaxies.

Many papers have been devoted to understanding the physical reason behind the K-S relation (e.g. Krumholz & McKee (2005)). However, it remains poorly understood. Since massive stars are mainly observed in the spiral arms of disk galaxies, it has been proposed that star formation is regulated by galactic shocks driven by spiral density waves (e.g. Binney and Tramaine (2008)) and by the increase of cloud-cloud collisions (Tasker & Tan (2009), Tasker (2011)). Krumholz & McKee (2005) propose a star formation model in which star formation efficiency depends on the turbulent properties of the molecular clouds and demonstrate that the Kennicutt-Schmidt relation can be explained by their model. Turbulent internal motion in clouds can be exited by cloud-cloud collisions via the conversion of the orbital energy of the clouds into internal motion energy (Bonnell et al. (2006), Dobbs et al. (2006), Tasker & Tan (2009) and Tasker (2011))

Barred galaxies show different star formation activity in the bar regions and in the spiral arms regions, even when gas surface density in both regions is comparable (e.g., Downes et al. (1996), Sheth et al. (2000), Muraoka et al.

© 2012 RAS

(2007), and Momose et al. (2010)). Studying the physical reason for this discrepancy is an important step to understanding the physics for the K-S relation.

It is well known that the star formation activity is higher in spiral arms regions than in the bar regions, even if the bar regions are gas rich (Momose et al. 2010). We focus on the possibility that this difference is related to a difference in cloud properties between these regions, since the cloud environment is thought to be closely related with SF (Krumholz & McKee (2005)).

Gas flows in the bar regions are elongated with strong shears and dark lanes that are evidence for strong shock waves(e.g. Wada & Habe (1992)). It is therefore natural to expect clouds forming in this environment to have different properties from elsewhere in the disk.

In this paper, we present a numerical simulation of gas flow at high resolution in a barred galaxy potential. We include cooling and heating processes and study the properties of clouds in different galactic environments within the disk and how this relates to star formation. For the purpose, we resolve gas clumps as large as molecular clouds.

As the first step in our study, we perform a two dimensional simulation with spacial resolution of 4 pc. The galaxy model is that of a barred galaxy with a bar similar to M83. M83 is one of the best targets to study the spacial variation of star formation efficiency in a barred galaxy, since it is nearby and has been well observed in various wave lengths, e.g., atomic gas (Huchtmeier & Bohnenstengel 1981), the molecular gas (Lundgren et al. (2004a), Sakamoto et al. (2004), Muraoka et al. (2007)), optical emission lines (Dopita et al. 2010), X-ray (Soria & Wu 2003).

From the physical properties of the identified clumps, we estimate the SFE and SFR, using the simple star formation model of turbulent clouds proposed by Krumholz & McKee (2005).

The plan of this paper is as follows: Section 2 describes our model and numerical method. In section 3, we show our numerical results. In section 4, we estimate SFR and SFE in the bar region and the arm region by using the simple model of Krumholz & McKee (2005). In section 5, we present our discussion and conclusion.

2 MODEL AND NUMERICAL METHOD

2.1 Model Galaxy

We use a gravitational potential for a barred galaxy similar to that of M83. This model is from the work of Hirota (2009) who analyzed the 2Mass K-band image of M83 (Jarrett et al. 2003), assuming a constant mass to light ratio. The model galaxy consists of stellar bulge, stellar bar, stellar disk and dark halo components. The circular rotation velocity of the gravitational potential that is shown in Figure 1 roughly agrees with the observation of molecular gas in M83 by Lundgren et al. (2004b). The observed rotation velocity of molecular gas is 150 km/s at 2 kpc from the center and 180 km/s at 3 kpc from the center (Lundgren et al. 2004b). In our simulations, we assume that initial gas rotates in the gravitational potential with a circular velocity that balances the axial averaged gravity of the barred galaxy.

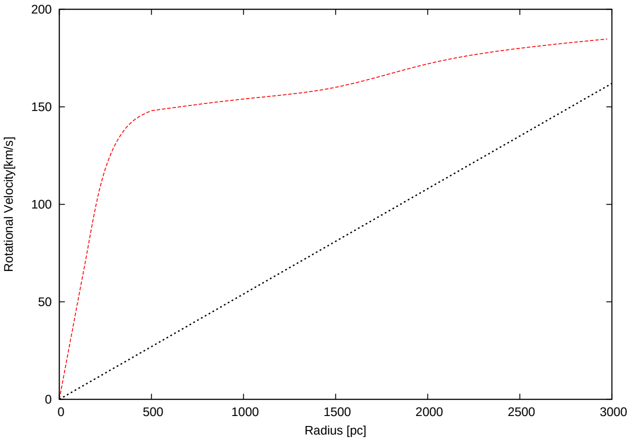

Figure 1. The circular velocity in the model galaxy and the pattern speed of the bar.

The pattern speed of the bar potential is $\Omega_p = 54$ km s^{-1} kpc^{-1}, in keeping with the observed global characteristics of the gas distribution in M83 (Hirota (2009), Hirota et al. (2009)). The parameters for the initial conditions of our simulations are shown in Table 1. For the initial radial distribution of gas mass surface density in the disk, we assume the Gaussian central component and the exponential gas disk component given by Lundgren et al. (2004a) (Fig. 2). The total gas mass within a radius of 7.3 kpc is $3.5 \times 10^9 M_\odot$.

2.2 Numerical Method

We simulate two dimensional gas flow in the model galaxy using our M-AUSMPW$^+$ code (Namekata & Habe 2011), which is based on an advection upstream splitting scheme (Kim & Kim 2005b) with the MLP5 (Kim & Kim 2005a) for calculating the higher oder numerical fluxes. The size of simulation region is 12.6 kpc × 12.6 kpc and covers the whole stellar disk of M83. The grid size in our simulation is 3125^2, with a cell size of 4 pc.

For the first 80 Myrs, we calculate gas motion assuming an isothermal, non self-gravitating gas with $T = 10^4$K. At this stage, gas density distribution is steady. After this time, we take into account radiative cooling, heating and self-gravity of the gas for the next 40 Myr, which is long enough for the formation of the molecular clouds. Self-gravity of the gas is calculated by FFT of which a detailed description is given in Namekata & Habe (2011). We do not include star formation processes or any stellar feedback throughout our simulation, as we are concentrating on the properties of the clouds formed in the bar galaxy potential. We use a cooling function of gas with a solar metallicity given by Spaans & Norman (1997). For the heating processes, we assume a uniform FUV radiation field and a uniform cosmic ray heating in the energy conservation equation in the numerical hydrodynamics. We use the far ultra-violet (FUV) heating rate $\Gamma_{\rm FUV} = 1.0 \times 10^{-24} \varepsilon G_0$ (Gerritsen and Icke 1997). We assume $\varepsilon = 0.05$ and $G_0 = 1.0$ (Huchtmeier & Bohnenstengel 1981). When radiative cooling is allowed, the gas is allowed to cool to 10 K. For calculation of the cooling rate, gas density is obtained by assuming the thickness of the gas disk is 70 pc.

Table 1. Simulation condition

simulation	grid points	initial mass	initial mass distribution
I	3125 × 3125	$3.4 \times 10^9 M_\odot$	Gaussian + exponential

$M_\odot$ is the solar mass.

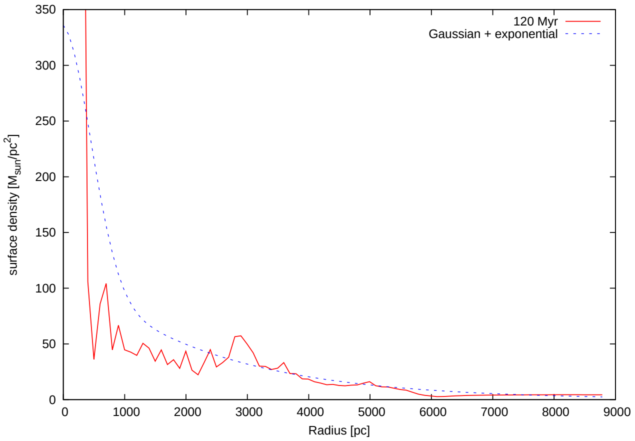

Figure 2. The azimuthally averaged gas surface density at t = 120 Myr (solid line). Dotted line is the initial gas distribution.

2.3 Clump finding method

In order to study the properties of clumps in the bar and spiral region, we identify clumps that are dense and have a low temperature by the following method: (A more detailed description is given in Namekata & Habe (2011)). First, cells with a surface density higher than $\Sigma_{\rm cl}$ and temperature lower than $T_{\rm cl}$ are selected as a 'candidate' clump member. Next, if a neighbouring cell to the 'candidate' is also a candidate, these cells become members of the same group. We iterate this procedure for all candidate cells. If cell number of a group exceeds $n_{\rm cl}$, the group is identified as a clump.

Since the mean surface gas density is less than $60{\rm M}_\odot/{\rm pc}^2$ except for where $r < 600$ pc, as shown in Figure 2, we assume $\Sigma_{\rm cl} = 60{\rm M}_\odot/{\rm pc}^2$ and $n_{\rm cl} = 12$. These values of $\Sigma_{\rm cl}$ and $n_{\rm cl}$ correspond to the lower limit mass of clumps of $m_{\rm cl} \sim 10^4 M_\odot$.

3 RESULTS

3.1 Disk gas evolution

Figure 3 shows the gas surface density distribution at the final stage of the isothermal gas simulation at t = 80 Myr. In this Figure, rotation of the gas and the bar pattern speed are in the counter-clock direction. The major axis of the bar is along the x-axis. Two dominant gas spirals extend from the bar ends and dense gas distributes in the bar region. We continue the simulation with cooling and heating processes and self-gravity of the gas, untill t = 120 Myr.

Figure 4 shows the gas surface density distribution at t = 120 Myr. Many irregular structures of dense gas have formed in the spiral and bar regions. In Figure 4, dense gas extends in the barred region more than in Figure 3 and the dense gas in the barred region shows dust-lane like features that extend away from the center and follow the inner edges of the spiral arms, similar to those observed in a barred galaxy. These dense gas features have a low temperature ($T <$ 100 K) and are similar to the previous studies (Wada & Norman (2001), Wada & Koda (2001)). From our numerical result as shown in Figure 4 we call a rectangular region (-2 kpc $< x <$ 2 kpc and -1 kpc$< y <$1 kpc) the bar region and a ring region between r = 2 kpc and r =4 kpc the spiral region.

There are many dense gas cells with $\Sigma > 60 M_\odot {\rm pc}^{-2}$ and $T <$ 100 K. Total number of the dense gas cells is 341,854 at t = 120 Myr.

We show the probability distribution function (PDF) of surface density in Figure 5. This plot excludes the galactic central region of $r <$ 500pc where there is a large concentration of gas. The Figure shows that the PDF rapidly changes from t =80 Myr to 100 Myr and is almost steady in $t \geqslant 100$ Myr in the range of Σ >10 $M_\odot/{\rm pc}^2$. The PDF in this stage is approximated by a log-normal form (Padoan & Nordlund (2002), Wada & Norman (2001)) in the range of $\Sigma > 100 M_\odot/{\rm pc}^2$. The following analysis focusses on the simulation results at t = 120Myr, since the time between t = 80 and t = 120 Myr is long enough to have allowed more than one free-fall time for a typical giant molecular cloud (GMC), e.g. $t_{ff} = \sqrt{3\pi/32G\rho} = 4.74(n_H/100{\rm cm}^{-3})^{-0.5}$Myr, and current estimates suggest that GMCs live between 1 and 2 free-fall times (e.g. McKee and Ostriker (2007), and references therin).

We show the radial distribution of the azimuthally averaged gas surface density at t = 120 Myr in Figure 2. There are gas concentrations in the galactic central region ($r <$ 500pc) and near the bar ends ($r \sim$ 3 kpc). These characteristic features agree with the observed radial profile of CO ($J = 1-0$) and CO ($J = 3-2$) in M83 (Muraoka et al. 2007), except for the central 500pc region.

3.2 Physical properties of the clumps

We select clumps from our numerical results by the method described in section 2.3. These clumps are in the mass range of $10^4 < M < 10^9 M_\odot$. The most massive clump is in $r <$ 100 pc from the galactic center. The total mass of the clumps is 1.7 $\times 10^9 M_\odot$ in the gas disk. The mass of the clumps in the bar region is $1.32 \times 10^9 M_\odot$ and in the arm region is 0.38 $\times 10^9 M_\odot$. The total number of clumps in the gas disk is 3122. The number of the clumps in the bar region is 495 and in the arm region is 2617.

We show a mass function of clumps in our numerical result at t = 120Myr in Figure 6. In this Figure, we plot the number of clumps with an equal spacing of $d \log_{10} M = 0.05$. From Figure 6, $dN/dM \propto M^{-1.75}$ in $M > 10^5 M_\odot$, since

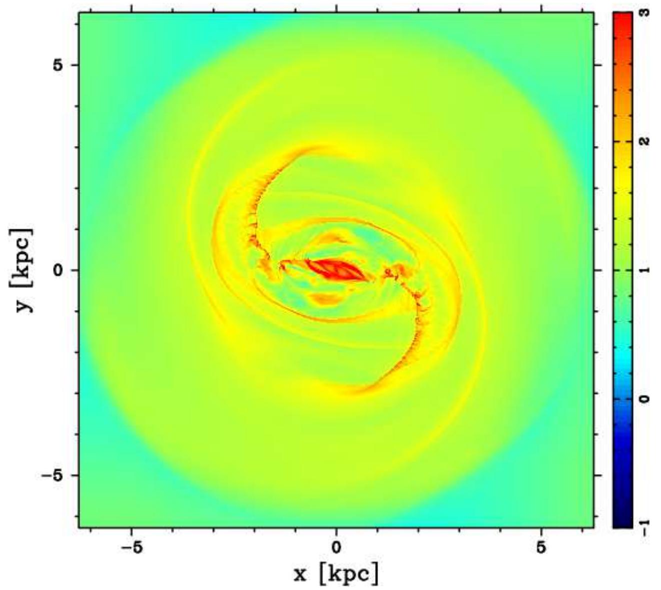

Figure 3. The gas surface density map at $t = 80$ Myr. Until this stage, gas is isothermal. The color bar in the right hand side shows the logarithmic scale of the surface density of gas in unit of $M_\odot$ pc^{-2}

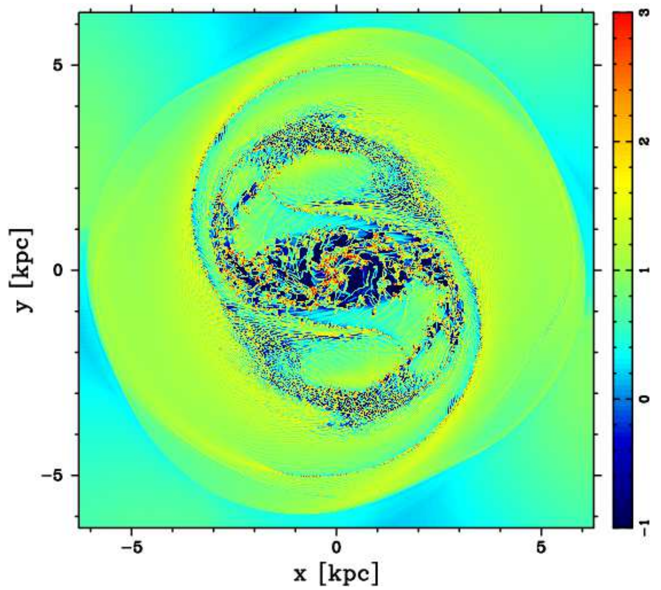

Figure 4. The same as figure 3, but for gas surface density map at $t = 120$ Myr. Our numerical simulation includes radiative cooling after $t = 80$Myr.

$$\frac{dN}{dM} = \frac{1}{M}\frac{dN}{d\ln M}. \tag{1}$$

This power index agrees well with the observed values ~ -1.5 in $M > 10^5 M_\odot$ in our Galaxy (Solomon et al. 1987). We test different thresholds of surface density for the clump finding method, and confirm that the power index of the clump mass function is almost independent from the choice of the threshold value.

We plot clump mass vs. their size in Figure 7. Plus symbols show clumps in the bar region. We use the color contour map to show clumps in the arm region which are too numerous to represent as points. The color bar shows number of clumps in the cell given by dividing the plot frame into 200 × 200. Since the clumps have an irregular shape, in this Figure, we estimate clump size l as:

$$l = ((\frac{S}{pc^2})/\pi)^{0.5} pc,$$

where S is area of the clump. Large size clumps of $l > 100$ pc are in the bar region and in the galactic central region ($r < 500$ pc). From Figure 7, we find the relation

$$M_{cl} = 10^{4.5}\ (l/10pc)^{2.5} M_\odot, \tag{2}$$

that is shown in Figure 7.

In Figure 8, we plot the one dimensional velocity dispersion, σ_v, of the internal velocity of the clumps vs. their sizes. σ_v is given by:

$$\sigma_v = \sqrt{\frac{1}{2m_{\rm cl}}\left(\sum_{i,j}\{\Sigma_{{\rm cl}\ i,j}(\boldsymbol{v}_{i,j} - \overline{\boldsymbol{v}_{\rm cl}})^2\}\right)} \tag{3}$$

from our numerical result, where $\Sigma_{{\rm cl}\ i,j}$ and $\boldsymbol{v}_{i,j}$ are the gas surface density and the velocity of gas in the (i,j) cell belonging to this clump, respectively. $\boldsymbol{v}_{cl}$ is velocity of the center of mass of this clump. Relation of the velocity dispersions and sizes of clumps is approximated as

$$\sigma_v = 0.8\ (l/1pc)^{0.5} km/s \tag{4}$$

in the arm region, which is shown by a dashed line in Figure 8. This relation is similar to the results of Larson (1981) and Solomon et al. (1987). Larson (1981) gives $\sigma_v = 1.1\ (l/1pc)^{0.38}$ km/s and Solomon et al. (1987) gives $\sigma_v = 1.0 \pm 0.1\ (l/1pc)^{0.5\pm0.05}$ km/s. There are clumps with larger velocity dispersions in the bar region than in the arm region. The@large velocity dispersion of clumps in the bar region may be due to their formation process; that is, clumps form from cooled gas in gas flow with strong shear motion in the bar region.

We plot internal velocity dispersion vs. mass of clumps in Figure 9. The relation between the internal velocity dispersion and the mass of clump is approximated as

$$\sigma_v = 2\ (M_{cl}/10^5 M_\odot)^{0.4-0.5} km/s. \tag{5}$$

The virial parameter is a useful measure of the gravitational stability of the clumps. Virial parameter of a spherical clump is given by

$$\alpha_{vir} = \frac{5\sigma_v^2 l}{GM_{\rm MC}}, \tag{6}$$

where $M_{\rm MC}$ is its mass, σ_v is its one dimensional velocity dispersion of internal motion, and l is its size. We modify α_{vir} as

$$\alpha_{vir} = \frac{10\sigma_v^2 l}{3GM_{\rm GMC}},$$

since our numerical calculation is two-dimensional. In Figure 10, we plot the virial parameter α_{vir} vs. mass of clumps. Several clumps in the bar region have larger virial parameters than in the spiral region. Number of clumps with $\alpha_{vir} > 1$ is 476 of the total 495 clumps in the bar and 2273 of the total 2617 clumps in the arm region. These gravitationally unbound clumps would be transient, since $\alpha_{vir} > 1$. Such transient clumps are found in the numerical simulation of giant

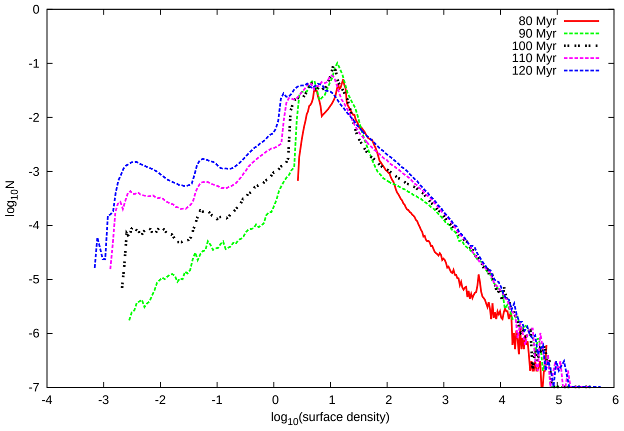

Figure 5. The PDF of surface gas density in unit of $M_{\odot}/\mathrm{pc}^{-2}$. We plot numerical results at $t = 80, 90, 100, 110$, and 120 Myr.

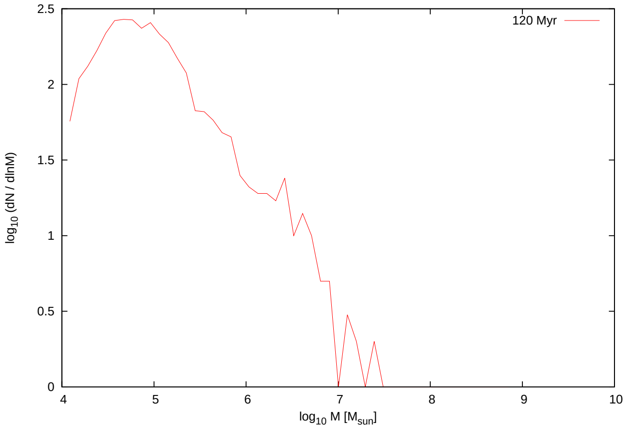

Figure 6. The clump mass function at $t = 120$ Myr.

molecular clouds formation by spiral shocks (Dobbs et al. 2006). In Dobbs et al. (2006), they show that a large part of the formed clouds are gravitational unbound and transient.@@ Mass fraction of clumps with $\alpha_{vir} < 1$ is 6.26% of the total mass of clumps in the disk. 0.14% of the total mass of clumps is in the bar region and 6.1% of the total mass of clumps is in the arm region. Fraction of clumps with $\alpha_{vir} < 1$ is much smaller in the bar than that in the spiral region. It is notable that clumps in the bar region are transient and the fraction of gravitationally unstable clumps is small, since these results can explain low star formation efficiency in the bar region.

We plot galactic radial distributions of velocity dispersion of clumps in Figure 11 and virial parameters of clumps in Figure 12. There are more clumps with large virial parameters in $r < 2.5$ kpc than that in $r > 2.5$ kpc. There are many clumps with $\alpha < 1$ in the spiral region. From these results, we expect many star forming clumps in these regions.

4 STAR FORMATION

We estimate the star formation rate from our numerical results. Since the cell size of our numerical simulation, 4 pc, is not enough to resolve the star formation process by hydrodynamical simulation, we use the star formation model proposed by Krumholz & McKee (2005) as sub-grid physics. In their model, they assume that star formation occurs in Jeans unstable parts of the giant molecular clouds and is regulated by the turbulent motions in the giant molecular clouds. In their model, they assume that turbulent velocities in the giant molecular clouds is described by a power law of the size of the turbulent motion, a probability density function for the density is a log normal type and star formation occurs in the Jeans unstable part of the giant molecular cloud. They obtain a star formation rate for a giant molecular cloud as:

$$SFR = SFR_{\mathrm{ff}} \frac{M_{\mathrm{GMC}}}{t_{\mathrm{ff}}} \tag{7}$$

where

$$t_{ff} = \sqrt{\frac{3\pi}{32 G\rho}} = 1.5 \left(\frac{n_H}{1000 \mathrm{cm}^{-3}} \right)^{-1/2} \mathrm{Myr}. \tag{8}$$

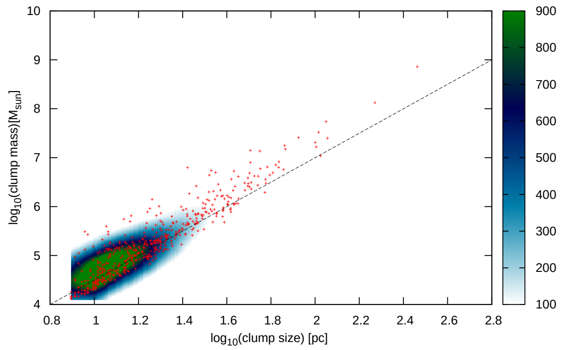

Figure 7. Clump mass vs. clump size for the clumps in our numerical results at $t = 120$ Myr. Plus symbols show clumps in the bar region and the color contour map shows clumps in the arm region. The color bar shows number of clumps in the cell given by dividing the plot flame into 200 × 200.

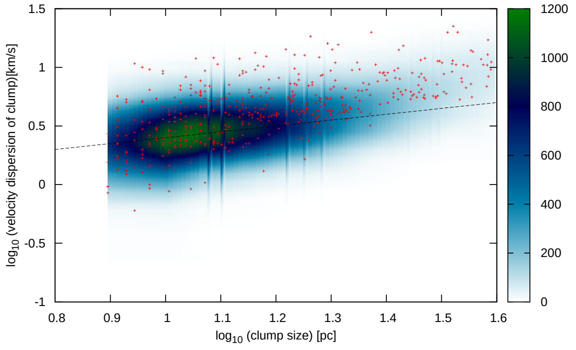

Figure 8. The same as Figure 7, but for the distribution of velocity dispersion of internal motion vs. clump size for the clumps in our numerical results at $t = 100$ Myr. The dashed line shows the relation given by Solomon et al. (1987)

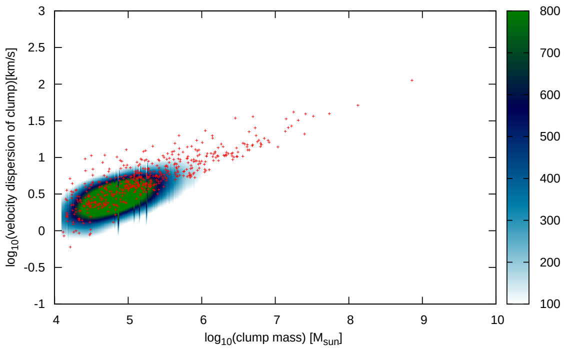

Figure 9. The same as Figure 7, but for the distribution of velocity dispersion of internal motion vs. clump mass for the clumps in our numerical results at $t = 120$ Myr.

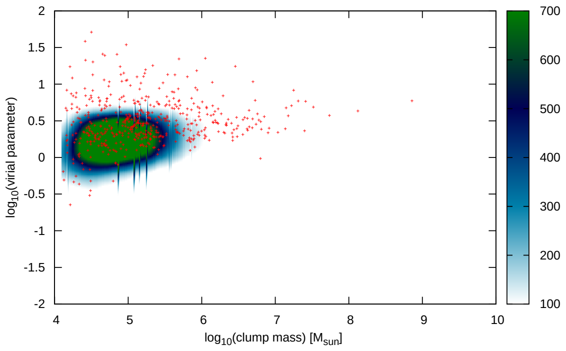

Figure 10. The same as Figure 7, but for the distribution of the virial parameter of clumps with clump mass at $t = 120$ Myr.

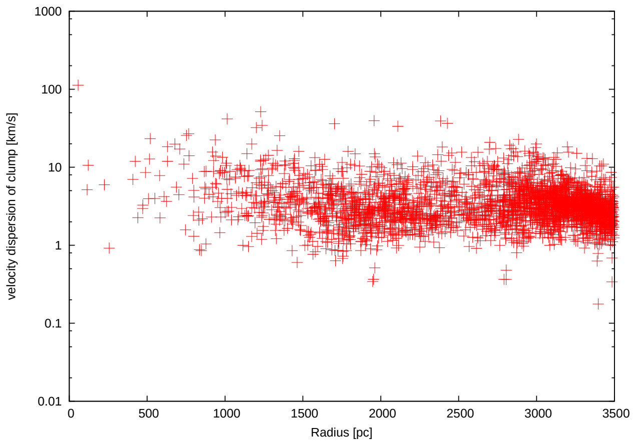

Figure 11. The radial distribution of velocity dispersion of clumps in the galaxy at $t = 120$ Myr.

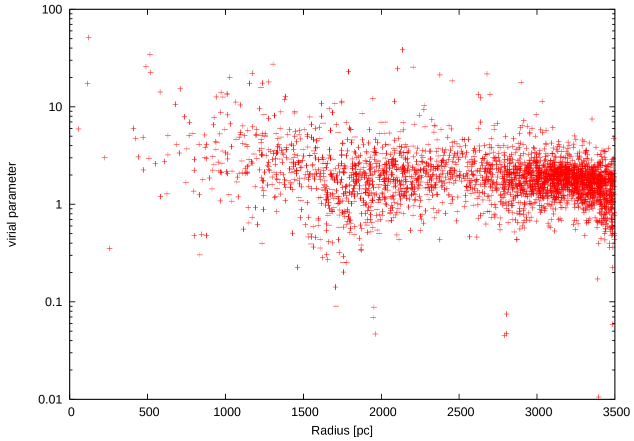

Figure 12. The radial distribution of virial parameter of clumps in the galaxy at $t = 120$ Myr.

and

$$\mathrm{SFR}_{\mathrm{ff}} = 0.014 \left(\frac{\alpha_{\mathrm{vir}}}{1.3}\right)^{-0.68} \left(\frac{\mathcal{M}}{100}\right)^{-0.32}, \qquad (9)$$

where $\mathcal{M} = \sigma_v / c_s$ and c_s is the sound speed of clouds. We estimate star formation rate in a clump as

$$\mathrm{SFR} = \left(\frac{\mathrm{SFR}_{\mathrm{ff}} f_{\mathrm{MC}} m_{\mathrm{cl}}}{t_{\mathrm{dyn}}}\right), \qquad (10)$$

where m_{cl} is the clump mass, f_{MC} is the fraction of molecular gas of it, and t_{dyn} is given by

$$t_{\mathrm{dyn}} = \frac{\sigma_v}{\pi G \overline{\Sigma}_{\mathrm{cl}}} = 1.36 \left(\frac{\sigma_v}{1\mathrm{km\ s}^{-1}}\right) \left(\frac{\overline{\Sigma}_{\mathrm{cl}}}{50 M_{\odot} \mathrm{pc}^{-2}}\right)^{-1} \mathrm{Myr}. (11)$$

$\overline{\Sigma}_{cl}$ is the mean surface density of each clump.

4.1 Relation of Star Formation Rate Surface Density and Gas Surface Density

We obtain a SFR from our numerical results by assuming that the SFR for each clumps@is given by equation (10) with $f_{\mathrm{MC}} = 1$, that is, the clumps are assumed to be mainly composed of H_2 molecules. We show the SFR surface density vs. surface density of mass of clumps over the average scale of 500 pc in Figure 13 (the arms region) and in Figure 14 (the bar region). These figures show that the SFR surface density is larger in the arms region than the bar region for the same clump mass surface density. Correlation shown in Figure 13 and Figure 14 agrees well with the relation given by Kennicutt (1998) and Bigiel et al. (2008).

4.2 Radial Distribution of Star Formation Rate

We show the radial distribution of the mean star formation rate surface density in Figure 15. In Figure 15, we exclude the central region of $r < 500$ pc, since there is high mass concentration of clumps and the star formation rate is very high in this region. The star formation rate between 0.5 kpc $< r <$ 2.5 kpc is $\Sigma_{\mathrm{SFR}} \sim 10^{-7.5} M_{\odot}/pc^2/yr$ which is smaller than $\sim 10^{-7.8} M_{\odot}/pc^2/yr$ in the region of 2.5 kpc $< r <$4 kpc. There is an enhancement of the star formation rate near $r =$3 kpc that is near the outside edge of the bar

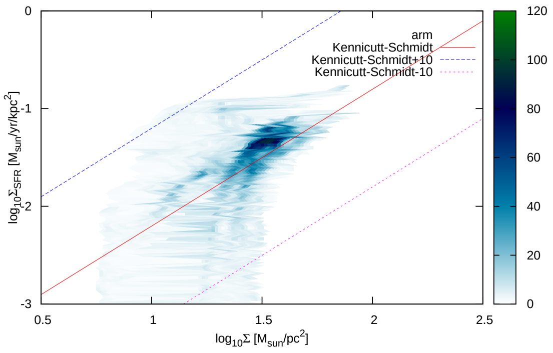

Figure 13. The distribution of the SFR surface density averaged in the scale of 500 pc with the clump mass surface density averaged in the same scale at $t = 120$ Myr in the arms region. The color bar shows number of cells of numerical hydrodynamic simulation. The red solid line shows the Kennicutt - Schmidt relation. The blue dotted line shows 10 times the Kennicutt - Schmidt relation. The magenta dotted line shows 1/10 the Kennicutt - Schmidt relation.

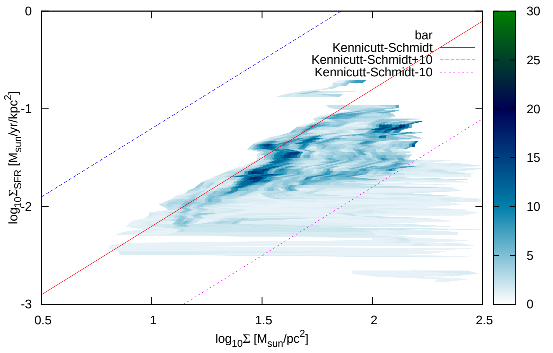

Figure 14. The same as in figure 13, but for the bar regions.

region. The star formation rate agrees with the estimation of Muraoka et al. (2007) within their uncertainty.

We show the radial distribution of star formation efficiency, i.e., star formation rate per unit clump mass, in Figure 16. In Figure 16, we also exclude the central region of $r < 500$ pc. The star formation efficiency in the bar region is three times smaller than the arm region. This trend is observed in barred galaxies (Muraoka et al. (2007), Momose et al. (2010)) . Our numerical results show that many more clumps in the bar region have large virial parameters with $\alpha > 1$ than in the arm region. This is the reason why the star formation efficiency is small in the bar region. In NGC 4303, SFE is larger than our numerical results with $\sim 10^{-8.5}$ yr^{-1} in bar region and $\sim 10^{-8.5} - 10^{-7.5}$ yr^{-1} in the arm region. This is because SFR is slightly higher in NGC 4303 than the mean value of the KS relation (Momose et al. 2010).

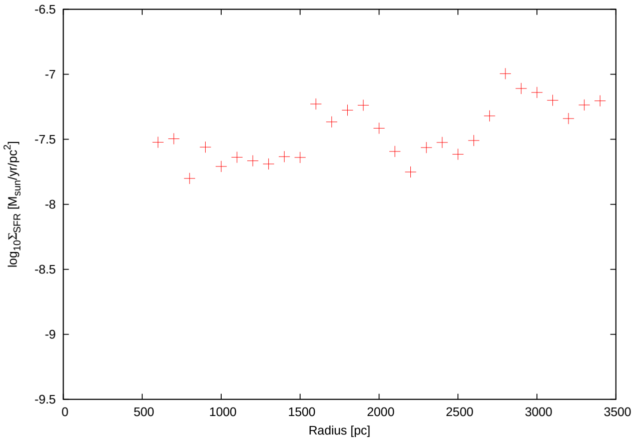

Figure 15. The radial distribution of star formation rate obtained by using the Kulmholts-McKee star formation model in the model galaxy . We show the star formation rate in $r \geqslant 600$ pc.

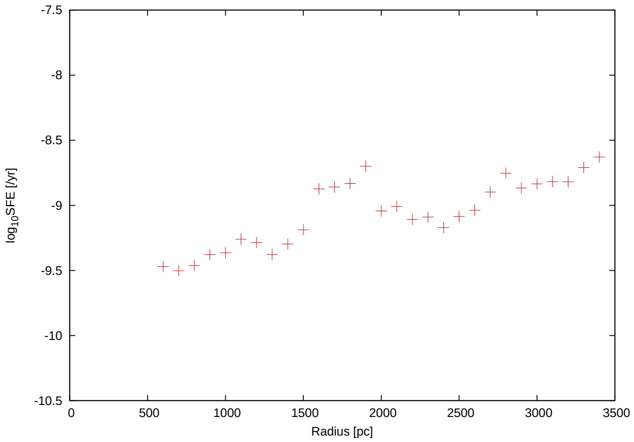

Figure 16. The radial distribution of star formation efficiency in $r > 600$pc..

5 DISCUSSION AND CONCLUSION

Our numerical results have shown that most of massive clumps in the bar region have large virial parameters, α and that mass fraction of bound clumps in the bar region is smaller than in the spiral region, although the mean surface gas density is larger in the bar region than in the arm region. Because of large shear gas flow in the bar region, most of clumps formed from gas in the bar region may have large internal gas motions as shown in Figure 11. This is the reason why the mass fraction of bound clumps in the bar region is smaller than in the spiral region.

The star formation rate estimation from our numerical results agrees well with the K-S relation as shown in section 4. In this analysis, we use the star formation model of Krumholz & McKee (2005) in which they assume that gravitationally unstable parts of the molecular clouds with small turbulent velocities form stars. In their model, they assume the scaling relation between turbulent velocities and turbulent sizes as in Larson (1981). In their model, SF rate is given by the gravitational unstable part mass divided by its free fall time. In our analysis, turbulent velocities of clump sizes are assumed to be the velocity dispersions of internal motions of clumps in our numerical results.

We have examined the radial distributions of star formation rate and star formation efficiency, since our estimation of star formation rate agrees well with the observed Kennicutt-Schmidt relation. Both radial distributions are within the error bars of observation of M83 (Muraoka et al. 2007) in $r > 1kpc$ and are smaller in the bar region than in the arm regions. The decrease of both quantities in the bar region is similar to the recent observations of barred galaxies (Momose et al. 2010). Our numerical results show that most of massive clumps in the bar region have large virial parameters, α and that mass fraction of bound clumps in the bar region is smaller than in the spiral region, although the mean surface gas density is larger in the bar region than in the arm region. Lundgren et al. (2004b) shows that molecular gas velocity dispersion is large in the bar region in M83. Sorai et al. (2012) shows that molecular gas in the bar in Maffei 2 has also large velocity dispersion. Lundgren et al. (2004b) estimated the Toomre unstable criteria of molecular gas and showed a large gas mass ratio to the critical mass of the Toomre instability in the bar region. However, there are few HII regions in the bar region, except for the central star burst region, while HII regions correlate with the value of the ratio in the outside of bar region. This means that Toomre instability argument is not sufficient to discuss SF rate in the bar region.

Our numerical results show that the turbulent star formation model can explain the property of star formation in barred galaxies. It is important to study observationally the difference in cloud properties in the bar and in the arm region. and the relation between cloud property and SF activity in various environments in galaxies using radio telescopes with high spatial resolution, e.g. ALMA, that will make it possible to resolve molecular clouds in extragalaxies.

In our simulation, we do not consider feedback from star formation. If we consider destruction of clouds by star formation, the distribution of dense clumps would be changed and concentrate near the dust lanes more than in the present numerical result. In order to consider feedback process from star formation, 3D numerical simulations are needed, since the destruction of molecular clouds and expansion of gas via heating of newly formed stars and supernovae can be simulated by three dimensional simulations (e.g. Tasker & Bryan (2006)).

6 ACKNOWLEGMENTS

We acknowledge Elizabeth Tasker for useful comments who read our manuscript very carefully and helped to improve this paper. We also acknowledge useful discussions with Masayuki Fujimoto, Tetsuhiro Minamidani, Naomasa Nakai, Junya Ito, Junichiro Enomoto and Takashi Ito. Numerical computations were carried out on Cray XT4 at Center for Computational Astrophysics, CfCA, of National Astronomical Observatory of Japan. This work was supported by a Grant-in-Aid for Specially Promoted Research 20001003 (AH).

REFERENCES

Bigiel, F.; Leroy, A.; Walter, F.; Brinks, E.; de Blok, W. J. G.; Madore, B.; Thornley, M. D. 2008,AJ. 136, 28

Binney, J. and Tremaine, S., Galactic Dynamics, second Ed., Princeton Series in Astrophysics, 2008

Bolatto, A. D.; Leroy, A. K.; Rosolowsky, E.; Walter, F.; Blitz, L. 2008, ApJ. 686, 948

Bonnell, I. A.; Dobbs, C. L.; Robitaille, T. P.; Pringle, J. E., 2006, MNRAS, 365, 37

Dobbs, C. L.; Bonnell, I. A.; Pringle, J. E. 2006, MNRAS. 371, 1663

Dopita, M. A.; Blair, William P.; Long, K. S.; Mutchler, M.; Whitmore, B. C.; Kuntz, K. D.; Balick, B.; Bond, H. E.; Calzetti, D.; Carollo, M.; and 16 coauthors 2010, ApJ. 710, 964

Downes, D.; Reynaud, D.; Solomon, P. M.; Radford, S. J. E. 1996, ApJ. 461, 186

Fujimoto, M. 1968, ApJ. 152, 391

Gerritsen, J. P. E.; Icke, V. 1997, A&Ap. 325, 972

Gnedin, N. Y.; Tassis, K.; Kravtsov, A. V. 2009, ApJ., 697, 55

Habing, H. 1968, Bull. Astron. Inst. Neth., 19, 421

Handa T., Sofue Y., Nakai N., 1991, IAUS, 146, 156

Heyer, M.; Krawczyk, C.; Duval, J.; Jackson, J. M. 2009, ApJ. 699, 1092

Hirota, 2009 Private communication.

Hirota, A.; Kuno, N.; Sato, N.; Nakanishi, H.; Tosaki, T.; Matsui, H.; Habe, A.; Sorai, K., 2009, PASJ, 61, 441

Huchtmeier, W. K.; Bohnenstengel, H.-D. 1981, A&Ap. 100, 72

Jarrett, T. H., Chester, T., Cutri, R., Schneider, S. E., & Huchra, J. P. 2003, AJ, 125, 525

Kennicutt,R.C.Jr. 1998, ApJ, 498, 541

Kim K. H., Kim C., 2005a, Journal of Computational Physics, 208, 527

Kim K. H., Kim C., 2005b, Journal of Computational Physics, 208, 570

Krumholz M. R., McKee C. F., 2005, ApJ, 630, 250

Larson, R. B., 1981, Royal Astronomical Society, Monthly Notices,194, 809.

Lundgren A. A., Wiklind T., Olofsson H., and Rydbeck G., 2004a, A&A, 413, 505

Lundgren, A. A.; Olofsson, H.; Wiklind, T.; Rydbeck, G. 2004b, A& A, 422, 865

Mckee,C.F. and Ostriker,E.C., ARA&A, 45, 565.

Momose, R.; Okumura, S. K.; Koda, J.; Sawada, T. 2010, ApJ. 721, 383

Muraoka, K.; Kohno, K.; Tosaki, T.; Kuno, N.; Nakanishi, K.; Sorai, K.; Okuda, T.; Sakamoto, S.; Endo, A.; Hatsukade, B.; and 7 coauthors, 2007, PASJ. 59, 43.

Muraoka, K.; Kohno, K.; Tosaki, T.; Kuno, N.; Nakanishi, K.; Sorai, K.; Sawada, T.; Tanaka, K.; Handa, T.; Fukuhara, M.; and 2 coauthors, 2009, ApJ. 706, 1213.

Namekata D. & Habe A., 2011, ApJ, 731, 57.

Padoan, P. & Nordlund, A. , 2002, ApJ. 576, 870

Ostriker, E. C.; McKee, C. F.; Leroy, A. K., 2010, ApJ. 721, 975

Rosolowsky, E. 2007, ApJ. 654, 240

Sakamoto, K.; Matsushita, S.; Peck, A. B.; Wiedner, M. C.; Iono, D., 2004, ApJ. 616, L59

Schmidt, M., 1959, ApJ., 129, 243.

Sheth, K.; Regan, M. W.; Vogel, S. N.; Teuben, P. J. 2000, ApJ. 532, 221

Soria, R.; Wu, K. 2003, A&Ap. 410, 53

Spaans M., Norman C. A., 1997, ApJ, 483, 87

Solomon, P. M., Rivolo, A. R., Barrett, J., & Yahil, A., 1987, ApJ, 319, 730

Sorai,K., Kuno,N., Nishiyama,K. Watanabe,Y., Matsui,H. Habe,A., Hirota,A., Ishihara,Y. and Nakai,N. 2012 PASJ, 64, 51

Tasker, E. J., 2011ApJ. 730, 11

Tasker, E. J.; Bryan, G. L., 2006, ApJ. 641, 878

Tasker, E. J.; Tan, J. C., 2009, ApJ., 700, 358

Wada, K.; Habe, A., 1992, MNRAS. 258, 82

Wada, Keiichi; Koda, Jin, 2001, PASJ, 53, 1163

Wada, Keiichi; & Norman, Colin A., 2001, ApJ, 547, 172